Title

Evolution of steady-state material properties during catalysis: Oxidative coupling of methanol over nanoporous Ag0.03Au0.97

Authors

Zugic, Branko
van Spronsen, Matthijs A
Heine, Christian
et al.

Publication Date

2019-12-01

DOI

10.1016/j.jcat.2019.08.041

Evolution of steady-state material properties during catalysis: Oxidative coupling of methanol over nanoporous $Ag_{0.03}Au_{0.97}$

Branko Zugic, Matthijs A. van Spronsen, Christian Heine, Matthew M. Montemore, Yuanyuan Li, Dmitri N. Zakharov, Stavros Karakalos, Barbara A. J. Lechner, Ethan Crumlin, Monika M. Biener, Anatoly I. Frenkel, Juergen Biener, Eric A. Stach, Miquel B. Salmeron, Efthimios Kaxiras, Robert J. Madix, and Cynthia M. Friend

Accepted manuscript (J. Catal. 380, 2019, 366–374)

Published journal article can be found via

https://doi.org/10.1016/j.jcat.2019.08.041

Evolution of steady-state material properties during catalysis: Oxidative coupling of methanol over nanoporous $Ag_{0.03}Au_{0.97}$

Branko Zugic,[a,1] Matthijs A. van Spronsen,[a,b,1†] Christian Heine,[b] Matthew M. Montemore,[c] Yuanyuan Li,[d] Dmitri N. Zakharov,[e] Stavros Karakalos,[a] Barbara A. J. Lechner,[b,2] Ethan Crumlin,[f] Monika M. Biener,[g] Anatoly I. Frenkel,[d,h] Juergen Biener,[g] Eric A. Stach,[e] Miquel B. Salmeron,[b] Efthimios Kaxiras,[c] Robert J. Madix,[c] and Cynthia M. Friend[a,c*]

[a]Department of Chemistry and Chemical Biology, Harvard University, Cambridge, MA 02138, USA
[b]Materials Sciences Division, Lawrence Berkeley National Laboratory, Berkeley, CA 94720, USA
[c]Paulson School of Engineering and Applied Sciences, Harvard University, Cambridge, MA 02138, USA
[d]Department of Materials Science and Chemical Engineering, Stony Brook University, Stony Brook, NY 11794, USA
[e]Center for Functional Nanomaterials, Brookhaven National Laboratory, Upton, NY 11973, USA
[f]Advanced Light Source, Lawrence Berkeley National Laboratory, Berkeley, CA 94720, USA
[g]Nanoscale Synthesis and Characterization Laboratory, Lawrence Livermore National Laboratory, Livermore, CA 94550, USA
[h]Chemistry Division, Brookhaven National Laboratory, Upton, NY 11973, USA

[1]These authors contributed to the work equally
[2]Present address: Department of Chemistry, Technical University of Munich, Lichtenbergstr. 4, 85748 Garching, Germany
[*]Corresponding Author: friend@fas.harvard.edu

Abstract

Activating pretreatments are used to tune surface composition and structure of bimetallic-alloy catalysts. Herein, the activation-induced changes in material properties of a nanoporous $Ag_{0.03}Au_{0.97}$ alloy and their subsequent evolution under steady-state CH_3OH oxidation conditions are investigated. Activation using O_3 results in AgO and Au_2O_3, strongly enriching the near-surface region in Ag. These oxides reduce in the O_2/CH_3OH mixture, yielding CO_2 and producing a highly Ag-enriched surface alloy. At the reaction temperature (423 K), Ag realloys gradually with Au but remains enriched (stabilized by surface O) in the top few nanometers, producing methyl formate selectively without significant deactivation. At higher temperatures, bulk diffusion induces sintering and Ag redistribution, leading to a loss of activity. These findings demonstrate that material properties determining catalytic activity are *dynamic* and that metastable (kinetically trapped) forms of the material may be responsible for catalysis, providing guiding principles concerning the activation of heterogeneous catalysts for selective oxidation.

Keywords

Nanoporous Au; diluted alloys; selective oxidation of CH_3OH; in situ/operando multimodal approach; metastability

1. Introduction

The quest for catalysis by design necessitates an understanding of how to generate and retain reactive sites for specific chemical reactions. This requires understanding of catalyst activation and how the material evolves under steady-state catalytic conditions. Ideally, catalysts will be active and highly selective for a specific reaction over extended periods of time.

Alloy catalysts have the added complexity that the distribution of atoms on or near the surface is likely to depend on activation as well as reaction conditions. Both the

surface composition and structure of alloy catalysts determine the reactivity as well as selectivity because of intrinsic differences in bonding and bond activation of different metals. Furthermore, at modest reaction temperatures, the stable surface structure is not necessarily the thermodynamic ground state but can be a metastable one that is kinetically trapped. Hence, there is an opportunity to *design* selective catalytic processes that exploit these metastable states and thus to develop principles that predict how to tune the surface composition and structure using specific activation procedures and steady-state conditions—reaction temperature, pressure, and the ratio of reactants.

Advances in microscopy [1–3] and spectroscopy [4] have enabled the direct interrogation of atomic-scale surface arrangements under functioning catalytic conditions. Such data provide critical input for the rational design of improved catalytic materials. The importance of this concept has recently been illustrated for several catalytic systems, including Cu-ZnO, [5] Pd-Zn, [6] Pt-Ni [7] and Pt-Co [8]. A recent study followed the shape of Au nanoparticles *in situ* at an O_2 pressure of 1 bar using TEM showing a shape transition from truncated octahedral to rounded upon cooling below 393 K, explained by the O_2(ads)-induced stabilization of the (110) facet [9].

Recently, structural and compositional rearrangements induced during the initial *activation*, i.e. oxidation with O_3, and the subsequent reduction of nanoporous (np) $Ag_{0.03}Au_{0.97}$ was demonstrated [10]. Nanoporous $Ag_{0.03}Au_{0.97}$ is a support-free Au alloy with small amounts of Ag, produced by selectively etching Ag from a Ag-rich AgAu alloy. After O_3 treatment, both Au and Ag are oxidized, forming a thin film of Au_2O_3 and AgO (Fig. 1). The surface also becomes substantially enriched in Ag, by ~30% compared to the bulk. This oxide layer does not selectively oxidize CH_3OH; rather, combustion occurs initially. Combustion subsides over the course of several hours and methyl formate is produced selectively [10,11]. In recent work, the oxide was titrated from the surface by exposure to either CO or CH_3OH [10]; however, the catalyst was not characterized in the critical steady-state condition, leaving the question of what the active phase of np $Ag_{0.03}Au_{0.97}$ is under steady-state reaction conditions unanswered.

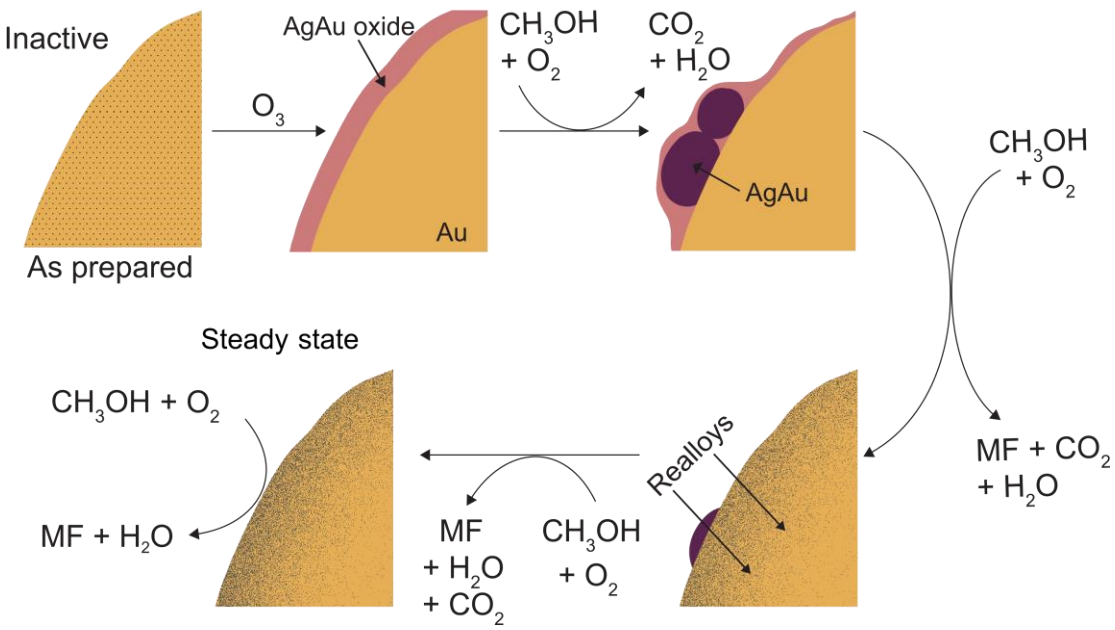

Fig. 1. Restructuring and redistribution of Ag at the surface of free-standing np $Ag_{0.03}Au_{0.97}$ under *steady-state conditions*, related to the high selectivity for methyl formate (MF) production. Exposure of the as-prepared catalyst to O_3 forms an oxide layer that is a few nanometers thick, with Ag concentrated in nanometer-scale patches on the surface. Under steady-state conditions, Ag redistributes into a silver-rich AgAu alloy that is kinetically confined to nanometer-scale regions near the surface. Dioxygen can be activated on these alloy regions, but requires multiple Ag atoms, based on DFT results. This work demonstrates the strong interplay between activation and kinetic trapping of a metastable state for steady-state catalytic function. The schematic is based on a combination of results from environmental transmission electron microscopy (E TEM), ambient-pressure X-ray photoelectron spectroscopy (AP XPS), and *operando* X-ray absorption fine-structure (XAFS) analysis. Color coding: Au matrix (dark yellow), Ag-rich regions (black speckles), AgAu oxide (pink), and AgAu alloy (dark purple).

Herein, the active phase of np $Ag_{0.03}Au_{0.97}$ under steady-state reaction conditions is identified for the first time and a metastable state is demonstrated to be responsible for prolonged *selective* catalytic oxidation of methanol (Fig. 1). Critical to the creation of this robust catalytic process is an aggressive pretreatment that dramatically alters the distribution of the minority metal, Ag, in the alloy by creating a surface oxide. During steady-state reaction, the Ag remains near the surface, forming a nanometer-scale metastable AgAu alloy that provides reactive sites for O_2 activation and ensuing selective oxidation. The ratio of Ag and Au on the surface varies as a function of temperature, time, and the O_2/CH_3OH ratio, creating a material in which active sites are present for selective reaction. The reactant composition and the temperature selected for reaction are critical to the stable function of the catalyst in this kinetically trapped, metastable state.

The results reported here for the steady-state catalyst demonstrate the complexity and the tunability of the alloy catalyst structure, composition and function by selecting appropriate activation and steady state reaction conditions. These results are a first step towards developing principles for designing catalytic processes that account for these factors.

2. Materials and Methods

Nanoporous AgAu alloys were created by dealloying AgAu bulk alloys in nitric acid. All samples had a residual Ag concentration of ~3 at.% after nitric acid leaching, as determined by energy-dispersive X-ray spectroscopy analysis. See supplementary information (SI), Section S1 for further details.

2.1 Ambient-pressure X-ray photoelectron spectroscopy (AP XPS)

The AP XPS experiments were conducted at beamline 9.3.2 at the Advanced Light Source at Lawrence Berkeley National Laboratory [12]. An O_3-treated np $Ag_{0.03}Au_{0.97}$ ingot (in a flow reactor in 2% O_3 in O_2 at 1 atm at 423 K for 1 h) was loaded onto a ceramic button heater, mounted in the AP XPS chamber. The mounted np $Ag_{0.03}Au_{0.97}$ sample was re-exposed to O_3 in the AP XPS chamber prior to analysis. An O_3 generator (Ozone Engineering LG-7) connected to ultra-high pure O_2 was used to generate a continuous O_3 stream (2% O_3 in O_2), which was dosed into the chamber to achieve a pressure of 0.3 Torr using a leak valve. The sample temperature was then increased to 423 K, and the sample was treated under these conditions for ~30 minutes. After O_3 treatment, the sample was cooled to room temperature, followed by evacuation to high vacuum. Oxygen (0.2 Torr) and methanol (0.1 Torr) were introduced into the chamber via leak valves. Methanol was introduced from a glass vial after the dissolved air was removed by freeze-pump-thaw cycles. During AP XPS, the pumping via the differentially pumped analyzer was compensated by continuously leaking in a small flow of O_2 and CH_3OH. The temperature was then ramped in 25 K increments to 423 K, and Au4f, Ag3d, O1s, and C1s spectra were collected at each temperature. See SI, Section S2 for analysis details.

2.2 X-ray Absorption Fine-Structure (XAFS) Spectroscopy

The Ag K-edge XAFS experiments were performed at beamline 2-2 at the Stanford Synchrotron Radiation Lightsource, SLAC National Accelerator Laboratory. Untreated, freshly dealloyed np $Ag_{0.03}Au_{0.97}$ foil samples were loaded into a quartz tube with an inner diameter of 0.9 mm and outer diameter of 1.0 mm and mounted onto a Clausen cell [13]. Samples were activated with 2–3 % O_3 in O_2 at 1 atm with a flow rate of 20 mL/minute and at 300–423 K for 2 h. Methanol oxidation was performed in 20% O_2 and 5% CH_3OH in He at 1 atm with a flow rate of 20 mL/minute. Data were collected in fluorescence mode. Photon-energy calibration was performed using reference data obtained for a Ag foil collected in transmission mode along with each scan (placed between ionization chambers downstream of the sample). Data analysis was performed using the IFEFFIT software package and the FEFF6 program [14]. For the Ag K-edge data, the fitting model includes two paths: Ag-Ag and Ag-Au. The energy shift, ΔE_0, under each condition was fixed to be the same for the Ag-Ag and Ag-Au paths. The amplitude reduction factor (S_0^2) for the Ag-M (M: Ag, Au) paths was obtained by fitting the data for the Ag foil (S_0^2=0.94). For the Ag edge data, the fitting *k* range was 2.0–11.0 $Å^{-1}$, and the fitting R range was 1.7–3.3 Å.

2.3 Environmental TEM (E TEM)

The E TEM facilities at the Center for Functional Nanomaterials at Brookhaven National

Laboratory were used. An aberration-corrected microscope (FEI Titan) was operated at 300 kV, with a base pressure of (3–4)×10^{-7} Torr and a spatial resolution of <180 pm. Ozone-treated np $Ag_{0.03}Au_{0.97}$ foils were suspended in deionized water by sonication and drop cast onto a sample holder (DENS Solutions). The sample was dried overnight at room temperature before being inserted into the microscope. Gases and vapors were admitted into the microscope through a gas-handling manifold equipped with dosing valves.

2.4 Density-Functional Theory (DFT)

Calculations were performed with the planewave VASP code [15,16], the projector-augmented wave method [17,18], and a 400-eV cutoff for the basis set. A 3×3 (111) surface cell with 4 layers was used, along with a k-point mesh of 7×7×1. Surface energies were calculated by referencing Au to bulk Au and Ag to a 2.1%-Ag-in-Au bulk alloy, and at each O coverage the surface energy of Au(111) was set to 0. Since only direct comparisons between surfaces with the same O coverage were made, a reference for O was not needed. For each case—Au(111), $^1/_3$ ML Ag, and AgAu nanoparticles—several O configurations were tested at each O coverage to find the most stable configuration. For the flat surfaces, some O configurations at high O coverage resulted in significant surface restructuring, creating rough structures somewhat similar to the nanoparticles. These rough structures were often more stable than flatter structures but were never as stable as the nanoparticle structures. Therefore, these rough structures were discarded so that the nanoparticle energies could be compared to the energies of flatter surfaces. Nanoparticles of varying compositions were evaluated, and the AgAu nanoparticle most stable at an O coverage ≥ 0.33 ML was compared to the flat surfaces. This nanoparticle is 66 at.% Ag, while the surface underneath the nanoparticle is pure Au. See SI, Section S3 for further details.

3. Results

3.1 Ambient-pressure X-ray photoelectron spectroscopy (AP XPS)

Both Ag and Au are oxidized after pretreatment of the np $Ag_{0.03}Au_{0.97}$ sample with O_3 (2% O_3, in O_2 at 1 atm and 423 K) even after intermediate exposure to air (Fig. 2.i), in agreement with prior work [10]. A single $Ag3d_{5/2}$ peak, characteristic of AgO [19,20], is observed at 367.2 eV (Table 1). The binding energy of oxidized Ag is lower than that for metallic Ag because of final-state effects [21]. The position is comparable with reported values of 367.1–367.2 eV after O_3 treating np Au [10,22,23] and the Au(111) single-crystal surface [24] with Ag as minority component. The $Au4f_{7/2}$ spectrum obtained after O_3 treatment has peaks characteristic of both metallic (84.0 eV) and oxidized Au (85.6 eV) (Fig. 2B.i). Previously, oxidized np Au led to a $Au4f_{7/2}$ peak at a position of +(1.3–1.6) eV relative to the metallic Au peak [22,23]. The intensity ratio of the peak areas, $I_{Au,oxide}/I_{Au,metallic}$, is 0.7, probed with an inelastic mean free path (IMFP) of 0.6 nm. With increasing IMFP, this ratio decreases (Fig. S7). Therefore, the fraction of Au oxide decreased gradually from the surface to deeper in the material.

Ex situ O_3 treatment strongly enriches the surface in Ag, based on the ratio of 1.5 for the I_{Ag3d}/I_{Au4f} ratio (Fig. 3). This ratio corresponds to ∼60 at.% Ag in the near-surface region or a concentration enhancement by a factor of 20 compared to the np $Ag_{0.03}Au_{0.97}$

bulk. *In situ* O_3 (1 Torr of O_3 in O_2 at 423 K) treatment further increased the I_{Ag3d}/I_{Au4f} ratio to 2.0. The Ag is highly enriched in the first few layers, below which is a region strongly depleted from Ag, based on the strong decrease of the I_{Ag3d}/I_{Au4f} ratio for longer IMFP of the photoelectrons (Fig. S8).

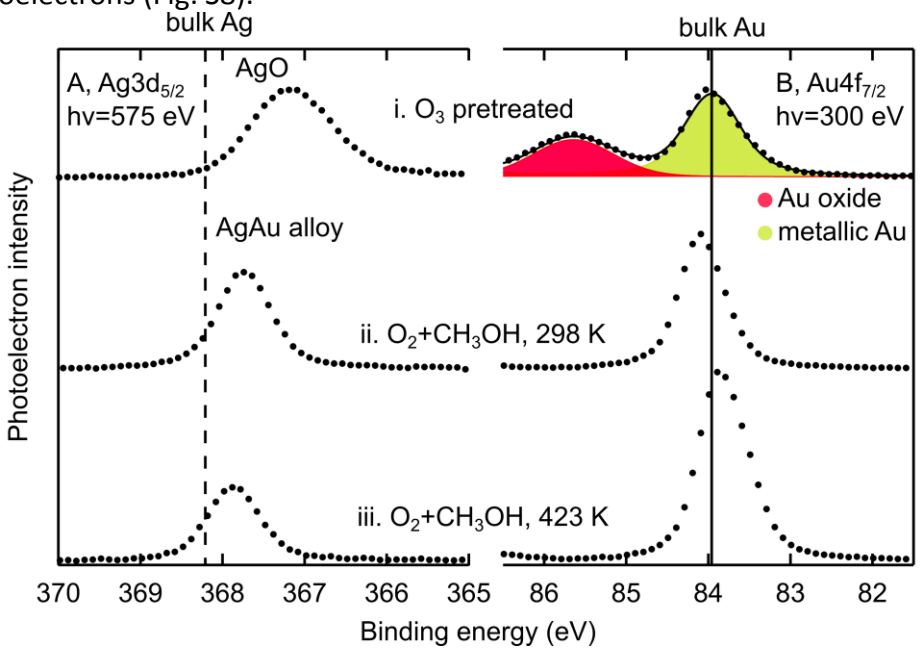

Fig. 2. X-ray photoelectron spectra of np $Ag_{0.03}Au_{0.97}$ show that the oxidation states and surface concentrations of Ag and Au depend on the temperature and gas environment. Spectra for the $Ag3d_{5/2}$ (A) and $Au4f_{7/2}$ (B) regions obtained under various conditions: (i) under ultra-high vacuum and at 298 K after *ex situ* treatment with O_3, showing the enrichment of the surface in Ag and the presence of AgO and a mixture of Au_2O_3 and Au; (ii) exposed to a mixture of O_2 and CH_3OH (0.2 and 0.1 Torr) at 298 K reducing both Ag and Au; the $Ag3d_{5/2}$ and $Au4f_{7/2}$ positions indicate alloy formation; (iii) heated to 423 K in O_2/CH_3OH resulting in a decrease of the Ag intensity. Inelastic mean free path of the photoelectrons was 0.6 nm [25], corresponding to 2–3 atomic layers of Au. Dashed (solid) line indicates position corresponding to bulk metallic Ag (Au) [26].

The *in situ* re-exposure to O_3 removed all adventitious carbon species (Fig. S9) present on the surface after loading the sample in the analysis chamber. Exposure to O_3 at much lower pressures, in the 10^{-7}-Torr range, also removed most C species from the surface of np Au [22]. If these C species were preferentially adsorbed on the Ag, then their removal also contributes to the further increase of the I_{Ag3d}/I_{Au4f} ratio observed after *in situ* O_3 treatment. After the O_3 treatment, a small amount of C-containing species reappeared on the surface stemming from adsorption of residual gas in the vacuum chamber (background pressure typically was in the order of 10^{-9} Torr).

Table 1. $Ag3d_{5/2}$ and $Au4f_{7/2}$ peak positions used to identify the state of Ag and Au in the nanoporous catalysts in comparison to reference data. Data for np $Ag_{0.03}Au_{0.97}$ were obtained for photon energies of 575 and 300 eV for $Ag3d_{5/2}$ and $Au4f_{7/2}$, respectively.

Material description	$Au4f_{7/2}$ / eV	$Ag3d_{5/2}$ / eV
O_3-treated np $Ag_{0.03}Au_{0.97}$	84.0; 85.5–85.6	367.0–367.2
Reduced np $Ag_{0.03}Au_{0.97}$	83.8–84.1	367.7–367.9
Pure, bulk metals	84.0[26]	368.2[26]
Au oxide	85.2[27]	
Bulk AgO		367.3[19,20]
Bulk Ag_2O		367.7[20]
Dilute Ag-in-Au alloy	83.8[28]	367.6–367.8[23,28]
Dilute Au-in-Ag alloy	84.1[28]	368.2[28]

The observed effect of the O_3 treatment is in general agreement with previous results [10], although the absolute values of the I_{Ag3d}/I_{Au4f} ratio are higher, *e.g.*, after *in situ* O_3 treatment, the I_{Ag3d}/I_{Au4f} ratio is 2 (Fig. 3) compared to 0.5 [10]. This may be related to local variations in the material composition or differences in the precise activation conditions. Moreover, the extent of Au oxidation was not as large as observed before, which may be attributed to the Ag oxide layer passivating the np $Ag_{0.03}Au_{0.97}$ from further oxidation.

Both Ag and Au reduce upon exposure to a mixture of O_2 (0.2 Torr) and CH_3OH (0.1 Torr) at room temperature (Fig. 2.ii), in agreement with prior work [10,23]. Reduction is indicated by the shift of the $Ag3d_{5/2}$ peak from 367.0 eV to 367.7 eV and the disappearance of the $Au4f_{7/2}$ oxide peak at 85.6 eV. The reduction commenced after the CH_3OH was added to the O_2 atmosphere and proceeded slowly at 298 K, requiring 10–20 minutes for complete reduction (Fig. S10). The presence of AgO supported on the Au surface, recently suggested to be the active phase for CO oxidation at room temperature [29], can be excluded.

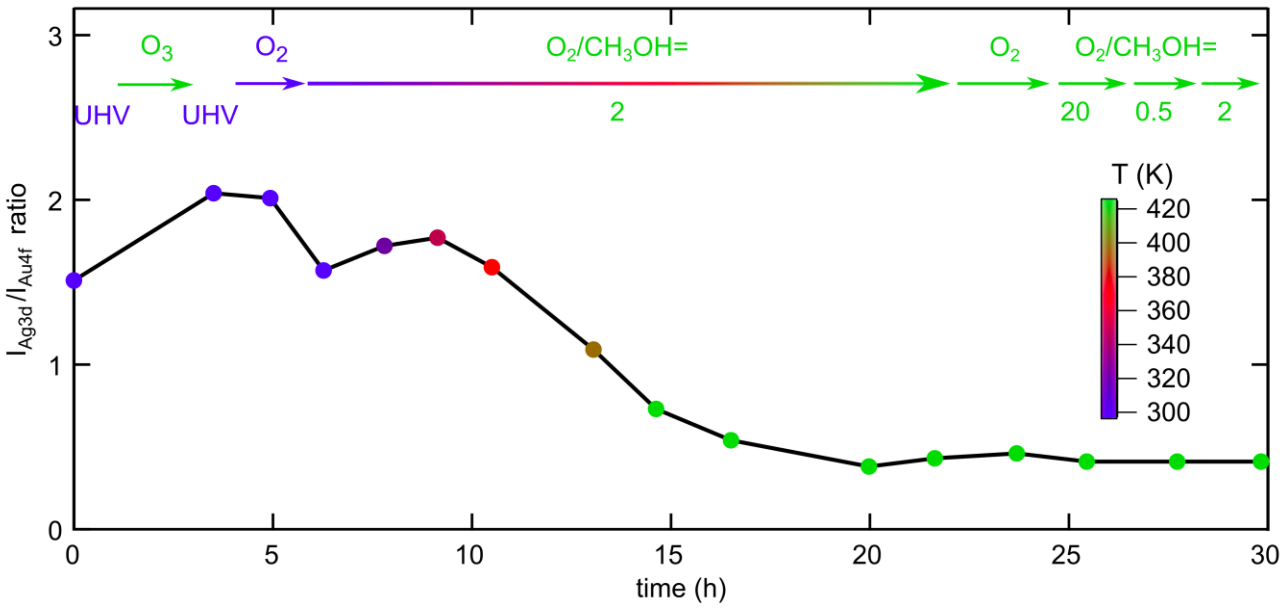

Fig. 3. Evolution of the ratio of the Ag3d to Au4f peak areas throughout the AP XPS experiment. Activation in O_3 enriches the surface in Ag; but Ag recedes into the surface forming a AgAu alloy under steady-state conditions for selective CH_3OH oxidation. The initial data point (t=0 h) was obtained under vacuum at 298 K for np $Ag_{0.03}Au_{0.97}$ after *ex situ* O_3 treatment. Subsequent *in situ* O_3 treatment at 423 K further increased the measured I_{Ag3d}/I_{Au4f} ratio. Exposure to 0.2 Torr O_2 at 298 K sustained the enrichment. Adding 0.1 Torr CH_3OH at 298 K led to a small decrease in I_{Ag3d}/I_{Au4f} ratio and reduction of the oxides, based on the $Ag3d_{5/2}$ and $Au4f_{7/2}$ core-level shifts (Fig. 2.ii). Sequential heating in the O_2/CH_3OH mixture leads to a strong decrease in the I_{Ag3d}/I_{Au4f} ratio starting at 348 K, reaching a steady-state value of ~0.4, under which conditions, the Ag is alloyed into the Au. After reaching steady state, changing the gas composition did not significantly influence the I_{Ag3d}/I_{Au4f} ratio. Color indicates temperature during experiment. See SI, Section S2 for analysis details.

The $Ag3d_{5/2}$ peak at 367.7 eV is ascribed to the formation of a AgAu alloy, based on the shift of −0.5 eV relative to bulk Ag (dashed line, Fig. 2A) and the absence of oxidic O in the O1s spectrum (Fig. S11). Similar Ag3d assignments were previously made for the state of Ag after reduction of O_3-activated np AgAu, based on the binding energy of 367.8 eV [23,24]. For nonporous AgAu alloys, negative $Ag3d_{5/2}$ core-level shifts of up to −0.6 eV with respect to that for pure Ag have been reported [28,30]. Although Ag_2O has a similar $Ag3d_{5/2}$ binding energy (367.7 eV) [20], its presence as a majority species can be excluded, because the oxidic O of Ag_2O would have led to a peak at 529.2 eV [20]; inconsistent with the observed O1s spectra (Fig. S11.ii).

After reduction by exposure to the O_2/CH_3OH mixture at 298 K, the I_{Ag3d}/I_{Au4f} ratio decreased from 2.0 to 1.6. This decrease is tentatively attributed to preferential adsorption of carbonaceous species to Ag. (Carbon-containing species accumulated under these conditions based on the C1s spectra, see Fig. S11.) The amount of carbon substantially decreased upon heating to 323 K and further decreased upon heating to 423 K, the steady-state reaction temperature (Figs S12 and S13). Correspondingly, the I_{Ag3d}/I_{Au4f} ratio increased from 1.6 at 298 K to 1.8 at 348 K.

Two competing factors affect the temperature dependence of the I_{Ag3d}/I_{Au4f} ratio: the amount of carbon and oxygen preferentially adsorbed on Ag and the surface concentration of Ag. Heating from 298 to 348 K led to a small increase in the I_{Ag3d}/I_{Au4f}

ratio, which correlates with a decrease in both C and O on the material (Figs S11–S13), and a decrease in attenuation of the Ag3d photoelectrons. Subsequent heating from 348 K to the steady-state reaction temperature of 423 K led to a decrease in the I_{Ag3d}/I_{Au4f} ratio, reaching a value of 0.7 after several hours, explained by Ag diffusion into the Au-rich bulk. Even at these modest temperatures, Ag and Au have enough mobility to restructure, as has recently been shown for the dramatic reconstruction of Au deposited on the Ag(110) surface at 400–425 K, much lower than the onset of bulk diffusion (~600 K) [31]. As Ag migrated into the bulk, the surface composition became predominantly rich in Au, explaining the $Au4f_{7/2}$ shift of −0.3 eV (Fig. 2.iii), typical for the surface core-levels shifts of Au4f [32–35]. Additionally, the $Ag3d_{5/2}$ peak shifted by +0.1 eV, possibly reflecting a change in the local Ag-Au coordination.

The I_{Ag3d}/I_{Au4f} ratio continued to decrease under constant reaction conditions, stabilizing after 5–7 h at 0.4 (Fig. 3). This corresponds to 29 at.% Ag, still an almost 10-fold enrichment with respect to the $Ag_{0.03}Au_{0.97}$ bulk. Changing the gas composition, including to pure O_2, did not affect the I_{Ag3d}/I_{Au4f} ratio, showing the necessity of using O_3 to activate the as-prepared np $Ag_{0.03}Au_{0.97}$ sample. The inability of O_2 to enrich the surface in Ag is related to the fact that Ag did not oxidize under these conditions (0.2 Torr O_2 and 432 K). This shows that oxidation is crucial to enriching the surface with Ag.

Under steady-state conditions, the surface of the catalyst is a Ag-enriched AgAu alloy containing adsorbed O with an O1s binding energy of 531.1–531.6 eV (Figs S11, S12). The I_{O1s}/I_{Au4f} ratio under these conditions was 0.5, very close to the I_{Ag3d}/I_{Au4f}, making the I_{O1s}/I_{Ag3d} ratio approximately 1. Other than the adventitious C present since after the O_3 treatment, the surface is under these conditions not populated with a measurable amount of C species.

3.2 Operando X-ray absorption fine structure (XAFS) studies.

Operando XAFS measurements probing the np $Ag_{0.03}Au_{0.97}$ bulk show that the Ag enrichment and the Ag oxidation during O_3 activation are not limited to the near-surface region. It corroborates that Ag is segregated during O_3 treatment and that Ag alloying with Au is promoted under reaction conditions at a pressure of 1 atm (Fig. 4). The Ag K-edge (25.5 keV) spectra were acquired at various stages of the activation process to follow local structural and chemical changes of the catalyst during O_3 treatment and evolution under selective CH_3OH oxidation conditions. A fresh np $Ag_{0.03}Au_{0.97}$ sample was characterized under the following conditions: in a flow of He prior to any treatment (298 K), in/after flowing O_3 (2% O_3 in O_2 at 1 atm) at 423 K, and under reaction conditions (20% O_2 and 5% CH_3OH in He at 1 atm and 298–423 K).

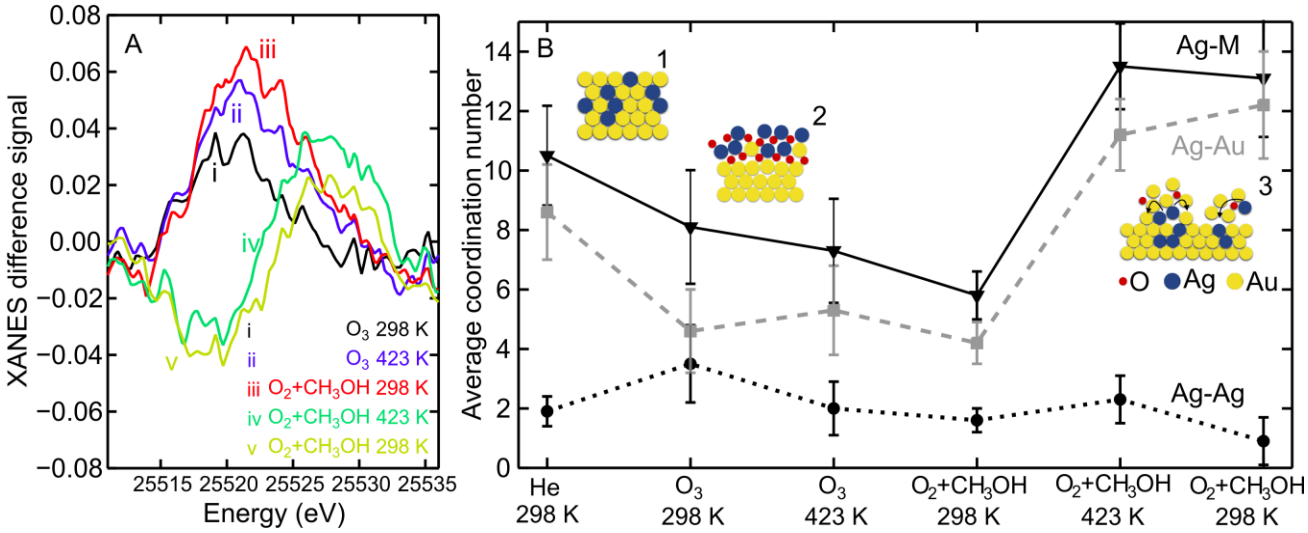

Fig. 4. XAFS of np $Ag_{0.03}Au_{0.97}$ during O_3 activation and exposure to CH_3OH oxidation conditions (A) Ag K-edge XANES difference spectra (as-prepared, nonactivated np $Ag_{0.03}Au_{0.97}$ in He at 298 K as reference) showing Ag oxide (i–iii) and its reduction by CH_3OH (iv and v). (B) Average Ag-Au, Ag-Ag, and Ag-M (M represents Au and Ag) coordination number derived from EXAFS. Activation in 2% O_3 in O_2 at 298–423 K (i and ii) and under/after reaction conditions (20% O_2 and 5% CH_3OH in He at 1 atm and 423 K). Inserts (B) show schematic representation of Ag redistribution within the np $Ag_{0.03}Au_{0.97}$ alloy: (1) as-prepared alloy; (2) O_3 treated with the surface oxidized and enriched in Ag; and (3) exposed to steady-state CH_3OH oxidation conditions with Ag realloying with Au but remaining near the surface. Atoms are indicated by red: O, blue: Ag, and yellow: Au.

The oxidation of Ag induced by the O_3 treatment is clearly demonstrated by intensity and position changes in the X-ray absorption near-edge structure (XANES) (Fig. **4**A). The XANES difference spectra show an increase in the Ag K-edge intensity and a shift to lower photon energy induced by the O_3 treatment. This is in line with the expected XANES contributions of Ag oxides compared to metallic Ag [36].

The Ag-Ag coordination number derived from the extended X-ray absorption fine structure (EXAFS) analysis (Fig. 4B) indicates that the distribution of Ag atoms in the as-prepared material is non-uniform. Therefore, the material contains regions with higher Ag content. The Ag-Ag coordination number is initially approximately 2 and the $N_{Ag\text{-}Ag}/N_{Ag\text{-}Au}$ ratio at all reaction conditions remains larger than $\frac{0.03}{0.97} \approx 0.03$, expected in a homogeneous random alloy [37,38]. The initial Ag-M coordination number of 11 hints that the Ag has a slight preference to be at the surface.

Segregation of Ag induced by the O_3 treatment is evident through the behavior of the Ag-Au and Ag-Ag coordination numbers. Fitting of the EXAFS signal under these conditions shows that the total Ag-metal (M) first-nearest-neighbor (1NN) coordination number decreased from approximately 11 (freshly prepared np $Ag_{0.03}Au_{0.97}$) to 6 as a result of the O_3 treatment, indicating the segregation of Ag from the np $Ag_{0.03}Au_{0.97}$ matrix. That decrease further suggests that Ag is brought to the surface, in line with the AP XPS and XANES measurements as well as with previous results [10].

Also in line with the AP XP results, dramatic changes in the Ag oxidation state and its coordination to Au are observed upon exposure to reaction conditions. The reduction of Ag is clearly observed in the XANES difference spectra as a decrease in peak intensity

relative to the initial reference condition (He at 298 K). The reduction in the K-edge intensity below the reference condition indicates that the sample is not only reduced but also distinct from the freshly dealloyed state. This further suggests a significant rearrangement of Ag within the np $Ag_{0.03}Au_{0.97}$ alloy during the activation process and can be explained by the dependence of the electronic structure of Ag on changes in its distribution.

3.3 Environmental Transmission Electron Microscopy (E TEM)

Electron-microscopy images evidence that the O_3-treated np $Ag_{0.03}Au_{0.97}$ alloy undergoes large-scale restructuring upon exposure to the O_2/CH_3OH reaction mixture (Fig. 5 and Movie S1). Immediately after O_3 treatment, the surface was covered with silver-rich oxides, consistent with previous work [10,39]. When O_2 (0.1 Torr) and CH_3OH (0.05 Torr) were introduced into the microscope, metallic nanoparticles rapidly formed on the surface under exposure to the electron beam. As the reaction proceeded, these particles were observed to realloy into the np $Ag_{0.03}Au_{0.97}$ ligaments (Fig. 5; Movie S1) over the course of ~6 minutes. The images shown were recorded at 298 K, in the presence of the electron beam; thermally induced realloying is much slower at 298 K, based on the slow change in selectivity from CO_2 to methyl formate that was attributed to this realloying, measured at 373–423 K at a pressure of 1 atm [10]. Regardless of the source of energy, the realloying process appears to be driven by reaction-induced diffusion occurring at the surface [40,41]. Importantly, the formation and alloying of particles did *not* occur under irradiation by the electron beam in the absence of reactants (Movie S2).

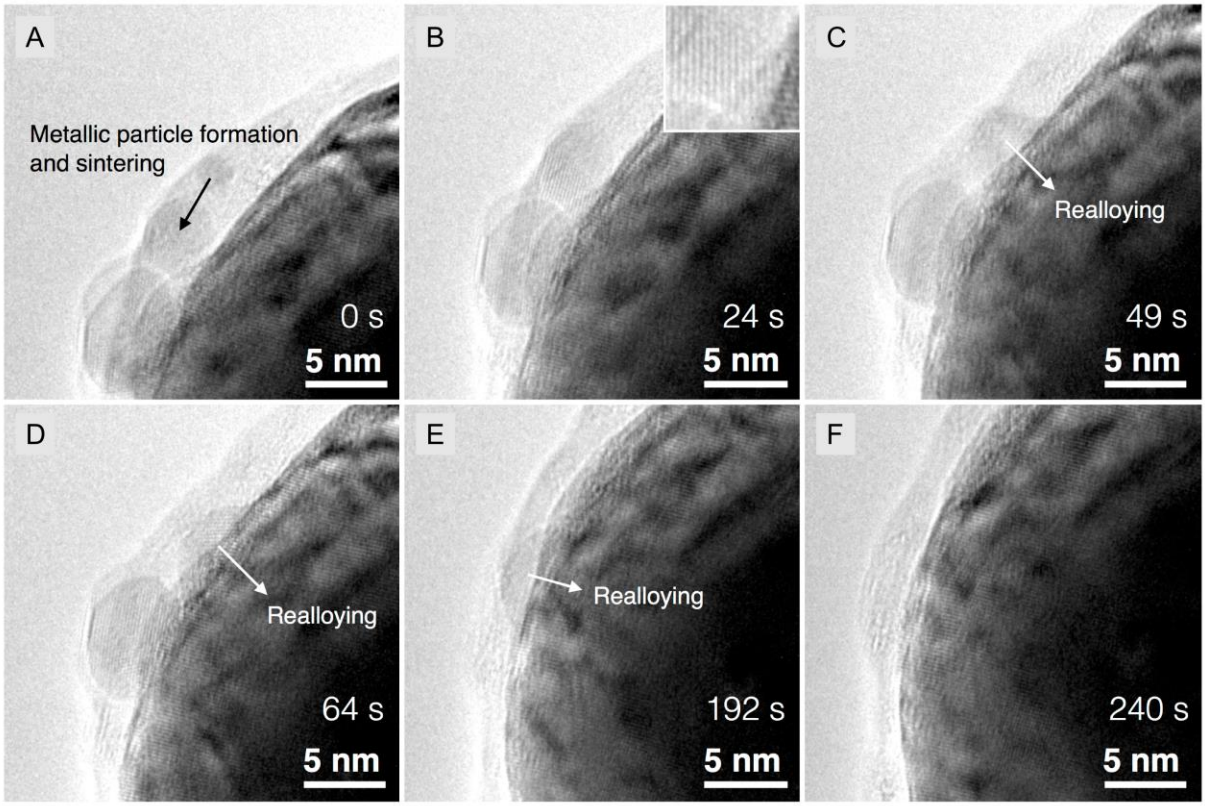

Fig. 5. E TEM images show changes in morphology of ligament edges associated with realloying of Ag into the np $Ag_{0.03}Au_{0.97}$ ligament. Snapshots from Movie S1 (SI, Section S5) of O_3-treated np $Ag_{0.03}Au_{0.97}$ to 0.1 Torr O_2 and 0.05 Torr CH_3OH at room temperature showing the realloying process that occurred over the course of 6 minutes. The catalyst was treated *ex situ* in O_3 in a flow reactor prior to loading onto the TEM grid. Insets show the metallic/crystalline nature of the nanoparticles formed from the oxide layer during reaction.

3.4 Density-Functional Theory (DFT)

The presence of ensembles of Ag in the near-surface region was previously shown to be critical for the initiation of the catalytic cycle through O_2 dissociation [42]. Multiple Ag atoms in close proximity are needed to reduce the activation energy for dissociation to a value near the desorption energy, even on rough surfaces—single Ag atoms are not sufficient [42–45]. Therefore, it is critical to have a significant amount of Ag on the surface, perhaps in localized regions, in order for the material to be catalytically active. To understand how O affects the surface composition, as well as its morphological structure, the energetic stabilities of two different Ag-containing structures relative to Au(111) were investigated. Necessarily, this model does not reflect the actual state of the catalyst because the calculations require a small, repeating lattice with Ag content that is considerably higher than the bulk average of 3%. In the catalyst material, the Ag is concentrated laterally by treatment with O_3 to create regions enriched in Ag (see above). Hence, the models are meant to provide insight into the types of local structures that may be present under reaction conditions.

Three model surfaces were considered: Au(111), Au(111) with 0.33 monolayer (ML) Ag in the surface layer (0.33 ML AgAu(111) alloy), and a model AgAu nanoparticle

(approximated by nanowire-like structures) (Fig. 6A). The Ag content in the two alloys was substantially higher than the overall bulk Ag concentration in order to more closely mimic the surface in the experiments. The model for the nanoparticle was simplified so as to be computationally tractable, while still accurately predicting qualitative trends applicable to larger nanoparticles (although these results may not be quantitatively accurate for determining the precise O coverage that results in nanoparticle formation). The DFT models included a structure of a Au surface oxide with an O coverage of 0.31 ML that had previously been identified as among the most stable Au-O surfaces in the literature [46].

The stability of surface structures with different geometries and Ag contents is strongly dependent on the oxygen coverage (Fig. 6B). On each of the three model surfaces, the oxygen coverage was varied from 0 to 1 ML. At the lowest O coverages, the Au(111)-terminated surface is marginally more energetically stable than the 0.33 ML Ag surface, as seen in previous work [47]. Experimental estimates of surface energies, derived from extrapolation of the liquid states, suggest that Ag has a lower surface free energy than Au [48]. Thus, one may expect Ag to segregate to the surface in AgAu alloys; however, the surface free energies of the components in the pure states are only moderately accurate as predictors of surface segregation in alloys, and the experimental surface free energies may have considerable errors. Further, there is evidence that surface segregation trends in AgAu alloys depend on the bulk composition [49]. Finally, entropy will favor diffusion of Ag into the nearly Ag-free bulk. Together, this shows that Ag enrichment is complicated, explaining why annealing in vacuum has been reported to both lead to Ag migration into the bulk [50] and Ag enrichement of the surface [51].

At low O coverages, the AgAu nanowire is most unstable (Fig. 6B) because of the low coordination of surface atoms. As the O coverage increases to ~0.2 ML, the stability of 0.33 ML AgAu(111) alloy approaches that of Au(111) and the energy of the nanowire decreases to be nearly the same as clean Au(111). At 0.31 ML O, the Au surface oxide is the most stable structure.

Of the structures considered, the AgAu nanowire is the most energetically stable for O coverages above 0.31 ML and is increasingly stable for higher O coverages (Fig. 6B). The AgAu nanowire is more stable by 0.9 eV per surface atom relative to the Au(111) surface at an O coverage of 0.9 ML. Notably, the 0.33 ML AgAu(111) alloy also decreases in energy at high O coverage (> 0.8 ML). Even so, the O-covered nanowire is more stable by ~0.3 eV at the highest O coverages and the surface substantially rearranges leading to a rougher surface morphology. Similarly, high O(ads) coverages can drive extensive restructuring of the pure Au surfaces, e.g. the flat Au(111) [52] and the stepped Au(321) surfaces [53].

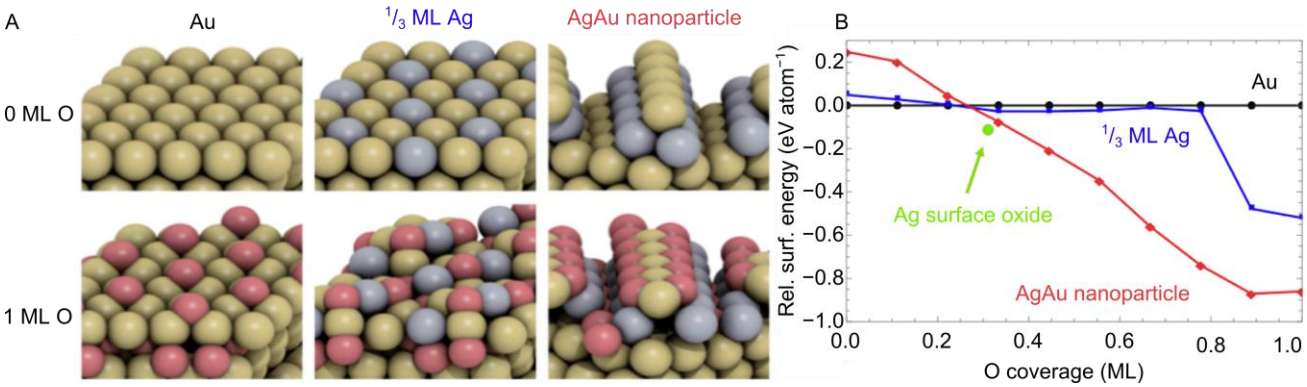

Fig. 6. The relative energetic stability of various surface terminations of two different AgAu alloy structures compared to Au(111) depends strongly on the O coverage based on DFT models.
(A) Schematics of the three lowest energy configurations of the three surfaces considered without O present (top) and with 1 ML of adsorbed O (bottom): Au(111), $Ag_{0.33}Au_{0.66}$/Au(111), and a nanowire-like AgAu alloy resembling nanoparticles. (B) Surface energies, per surface atom, of these models relative to pure, flat Au(111). The stability of a Au surface oxide with an O coverage of 0.31 ML is represented by the green dot.

These results indicate that a substantial O coverage is needed to bring a significant amount of Ag to the surface. The O_3 treatment provides this high O coverage, which also results in the formation of Ag-rich nanoparticles on the surface. Because bulk diffusion is slow in metals at moderate temperatures in the absence of a vacancy source [47], Ag is unlikely to diffuse far into the bulk under reaction conditions, once the Ag is in the surface region. Entropy was not considered in these calculations. Since the bulk Ag concentration is low, entropy would tend to drive Ag to the bulk, further supporting the conclusion that at low O coverage the surface is predominantly Au.

4. Discussion

The activation of the np $Ag_{0.03}Au_{0.97}$ alloy by oxidation in O_3 leads to a fundamentally different catalytic material compared to the as-prepared material (top left panel, Fig. 1). The formation of AgO drives enrichment in Ag in the surface region (top middle panel, Fig. 1). Enrichment in Ag of the surface of AgAu alloys has been observed before by exposure to O_3 [22,47], atomic O [50], or even O_2 at sufficiently high pressures [51]. To some extent, also Au oxidizes. Furthermore, O_3 treatment removes adventitious carbon from the surface.

Although the oxidized np $Ag_{0.03}Au_{0.97}$ has very poor selectivity in CH_3OH oxidation, mainly resulting in combustion, the oxides are unstable under reaction conditions. The reduction produces a surface AgAu alloy highly enriched in Ag. The Ag enrichment decreases with increasing temperature as the enhanced mobility allows Ag to realloy with the np $Ag_{0.03}Au_{0.97}$ bulk, similar behavior was observed after exposing O_3-treated np Au to CH_3OH oxidation conditions overnight [23].

Diffusion of Ag into the bulk is an important step because pure Ag is not a very selective catalyst for CH_3OH oxidation. The oxidation and realloying processes do not transpire homogeneously on the surface. After oxidation, oxide particles cover the

surface, which reduce into particles, before realloying more deeply into the subsurface in locally confined pockets (E TEM, Fig. 5).

Silver is crucial for O_2 activation [54], but AgAu islands, as observed in E TEM and AP XPS, are required for O_2 activation to initiate the catalytic cycle. Previous DFT studies have indicated that isolated Ag atoms are insufficient for O_2 activation but that larger Ag ensembles or AgAu alloy sites can enhance O adsorption [42–44,55]. The steady-state O coverage is considerable and can assist in stabilizing some of the Ag at the surface, as has been predicted for O(ads) on the Ag/Au(321) surface [50].

The modest steady-state reaction temperature is crucial because it prevents bulk diffusion, which would make Ag diffuse into the np $Ag_{0.03}Au_{0.97}$ bulk on a large scale. Moreover, it would promote sintering of ligaments, thereby reducing the surface area. Even at this modest temperature some sintering was observed under CH_3OH oxidation conditions [23]. Sintering can lead to irreversible loss of catalytic activity, as is observed for CO oxidation over np Au [54,56,57], for which the exothermicity of the reaction has been proposed to contribute to the coarsening [58].

The formation of a Ag-rich AgAu alloy suggests that a precise nanometer-scale structure and composition is required for selective oxidation. Recent reported results on AgAu nanoparticles embedded in a porous SiO_2 support this concept, showing that this behavior is not unique to the np $Ag_{0.03}Au_{0.97}$ alloy [59].

5. Conclusions

The combination of advanced characterization techniques and theoretical calculations demonstrates the importance of the dynamic rearrangement of bimetallic surfaces *during reaction* in the creation of active sites. Furthermore, the local geometrical and compositional nature of these sites is essential to their catalytic function. The oxidation of the np $Ag_{0.03}Au_{0.97}$ alloy by O_3 and its reduction under CH_3OH oxidation conditions initiate large-scale structural changes, which control the oxygen species present on the surface and their concentrations. These oxygen concentrations are correlated directly to the catalyst selectivity, allowing a better understanding of the nature of the surface alloy that is necessary to drive selective alcohol oxidation. Similar dynamics will be present in many bimetallic systems, and the current study emphasizes the importance of understanding their nature in order to fully unlock their catalytic potential.

Declaration of Competing Interest

The authors declare that they have no known competing financial interests or personal relationships that could have appeared to influence the work reported in this paper.

Acknowledgements

This work was supported as part of the Integrated Mesoscale Architectures for Sustainable Catalysis, an Energy Frontier Research Center funded by the U.S. Department of Energy, Office of Science, Basic Energy Sciences under award #DE-SC0012573. It also used resources (beamline 9.3.2) of the Advanced Light Source, which is supported by the Office of Science of the U.S. DOE under Contract No. DE-AC02-05CH11231. Work at LLNL was performed under the auspices of the U.S. Department of Energy by LLNL under

Contract DE-AC52-07NA27344. This research used resources of the Center for Functional Nanomaterials, which is a U.S. DOE Office of Science Facility, at Brookhaven National Laboratory under Contract No. DE-SC0012704. AIF and YL acknowledge the support from the U.S. Department of Energy Grant No. DE-FG02-03ER15476. Use of the Stanford Synchrotron Radiation Lightsource, SLAC National Accelerator Laboratory, is supported by the U.S. Department of Energy, Office of Science, Office of Basic Energy Sciences under Contract No. DE-AC02-76SF00515. We acknowledge the support at the BL2-2 beamline of the SSRL by the Synchrotron Catalysis Consortium (U.S. Department of Energy, Office of Basic Energy Sciences, Grant No. DE-SC0012335).

Appendix A. Supplementary material

Supplementary data to this article can be found online at https://doi.org/10.1016/j.jcat.2019.08.041.

References

[1] C.T. Herbschleb, P.C. Van Der Tuijn, S.B. Roobol, V. Navarro, J.W. Bakker, Q. Liu, D. Stoltz, M.E. Cañas-Ventura, G. Verdoes, M.A. Van Spronsen, M. Bergman, L. Crama, I. Taminiau, A. Ofitserov, G.J.C. Van Baarle, J.W.M. Frenken, The ReactorSTM: Atomically resolved scanning tunneling microscopy under high-pressure, high-temperature catalytic reaction conditions, Rev. Sci. Instrum. 85 (2014) 083703. doi:10.1063/1.4891811.

[2] S.B. Roobol, M.E. Cañas-Ventura, M. Bergman, M.A. van Spronsen, W.G. Onderwaater, P.C. van der Tuijn, R. Koehler, A. Ofitserov, G.J.C. van Baarle, J.W.M. Frenken, The ReactorAFM: Non-contact Atomic Force Microscope Operating under High-Pressure and High-Temperature Catalytic Conditions, Rev. Sci. Instrum. 86 (2015) 033706. doi:http://dx.doi.org/10.1063/1.4916194.

[3] J.F. Creemer, S. Helveg, G.H. Hoveling, S. Ullmann, A.M. Molenbroek, P.M. Sarro, H.W. Zandbergen, Atomic-Scale Electron Microscopy at Ambient Pressure, Ultramicroscopy. 108 (2008) 993–998. doi:http://dx.doi.org/10.1016/j.ultramic.2008.04.014.

[4] F.D. Ogletree, H. Bluhm, E.D. Hebenstreit, M. Salmeron, Photoelectron spectroscopy under ambient pressure and temperature conditions, Nucl. Instruments Methods Phys. Res. Sect. A Accel. Spectrometers, Detect. Assoc. Equip. 601 (2009) 151–160. doi:10.1016/j.nima.2008.12.155.

[5] M. Behrens, F. Studt, I. Kasatkin, S. Kühl, M. Hävecker, F. Abild-Pedersen, S. Zander, F. Girgsdies, P. Kurr, B.-L. Kniep, M. Tovar, R.W. Fischer, J.K. Nørskov, R. Schlögl, The active site of methanol synthesis over $Cu/ZnO/Al_2O_3$ Industrial catalysts, Science. 336 (2012) 893–897.

[6] K. Föttinger, J.A. van Bokhoven, M. Nachtegaal, G. Rupprechter, Dynamic Structure of a Working Methanol Steam Reforming Catalyst: In Situ Quick-EXAFS on Pd/ZnO Nanoparticles, J. Phys. Chem. Lett. 2 (2011) 428–433. doi:10.1021/jz101751s.

[7] D. Liu, Y. Li, M. Kottwitz, B. Yan, S. Yao, A. Gamalski, D. Grolimund, O. V. Safonova, M. Nachtegaal, J.G. Chen, E.A. Stach, R.G. Nuzzo, A.I. Frenkel, Identifying Dynamic Structural Changes of Active Sites in Pt–Ni Bimetallic Catalysts Using Multimodal Approaches, ACS Catal. 8 (2018) 4120–4131. doi:10.1021/acscatal.8b00706.

[8] H.L. Xin, S. Alayoglu, R. Tao, A. Genc, C.-M. Wang, L. Kovarik, E.A. Stach, L.-W. Wang, M. Salmeron, G.A. Somorjai, H. Zheng, Revealing the Atomic Restructuring of Pt–Co Nanoparticles, Nano Lett. 14 (2014) 3203–3207. doi:10.1021/nl500553a.

[9] A. Chmielewski, J. Meng, B. Zhu, Y. Gao, H. Guesmi, H. Prunier, D. Alloyeau, G. Wang, C. Louis, L. Delannoy, P. Afanasiev, C. Ricolleau, J. Nelayah, Reshaping Dynamics of Gold Nanoparticles under H_2 and O_2 at Atmospheric Pressure, ACS Nano. 13 (2019) 2024–2033. doi:10.1021/acsnano.8b08530.

[10] B. Zugic, L. Wang, C. Heine, D.N. Zakharov, B.A.J. Lechner, E.A. Stach, J. Biener, M. Salmeron, R.J. Madix, C.M. Friend, Dynamic restructuring drives catalytic activity on nanoporous gold–silver alloy catalysts, Nat. Mater. 16 (2017) 558–564. doi:10.1038/nmat4824.

[11] M.L. Personick, B. Zugic, M.M. Biener, J. Biener, R.J. Madix, C.M. Friend, Ozone-Activated Nanoporous Gold: A Stable and Storable Material for Catalytic Oxidation, ACS Catal. 5 (2015) 4237–4241. doi:10.1021/acscatal.5b00330.
[12] M.E. Grass, P.G. Karlsson, F. Aksoy, M. Lundqvist, B. Wannberg, B.S. Mun, Z. Hussain, Z. Liu, New ambient pressure photoemission endstation at Advanced Light Source beamline 9.3.2, Rev. Sci. Instrum. 81 (2010) 053106. doi:10.1063/1.3427218.
[13] P.J. Chupas, K.W. Chapman, C. Kurtz, J.C. Hanson, P.L. Lee, C.P. Grey, A versatile sample-environment cell for non-ambient X-ray scattering experiments, J. Appl. Crystallogr. 41 (2008) 822–824. doi:10.1107/S0021889808020165.
[14] M. Newville, IFEFFIT: interactive XAFS analysis and FEFF fitting, J. Synchrotron Radiat. 8 (2001) 322–324. doi:10.1107/S0909049500016964.
[15] G. Kresse, J. Hafner, Ab initio molecular dynamics for liquid metals, Phys. Rev. B. 47 (1993) 558–561. doi:10.1103/PhysRevB.47.558.
[16] G. Kresse, J. Furthmüller, Efficiency of ab-initio total energy calculations for metals and semiconductors using a plane-wave basis set, Comput. Mater. Sci. 6 (1996) 15–50. doi:10.1016/0927-0256(96)00008-0.
[17] P.E. Blöchl, Projector augmented-wave method, Phys. Rev. B. 50 (1994) 17953–17979. doi:10.1103/PhysRevB.50.17953.
[18] G. Kresse, D. Joubert, From ultrasoft pseudopotentials to the projector augmented-wave method, Phys. Rev. B. 59 (1999) 1758–1775. doi:10.1103/PhysRevB.59.1758.
[19] G.B. Hoflund, J.F. Weaver, W.S. Epling, AgO XPS Spectra, Surf. Sci. Spectra. 3 (1994) 163–168. doi:10.1116/1.1247779.
[20] G.B. Hoflund, Z.F. Hazos, G.N. Salaita, Surface characterization study of Ag, AgO, and Ag_2O using X-ray photoelectron spectroscopy and electron energy-loss spectroscopy, Phys. Rev. B. 62 (2000) 11126–11133. doi:10.1103/PhysRevB.62.11126.
[21] H. Grönbeck, S. Klacar, N.M. Martin, A. Hellman, E. Lundgren, J.N. Andersen, Mechanism for reversed photoemission core-level shifts of oxidized Ag, Phys. Rev. B. 8520 (2012) 115445. doi:10.1103/PhysRevB.85.115445.
[22] A. Schaefer, D. Ragazzon, A. Wittstock, L.E. Walle, A. Borg, M. Bäumer, A. Sandell, Toward controlled modification of nanoporous gold. A detailed surface science study on cleaning and oxidation, J. Phys. Chem. C. 116 (2012) 4564–4571. doi:10.1021/jp207638t.
[23] J. Dou, Y. Tang, L. Nguyen, X. Tong, P.S. Thapa, F.F. Tao, Oxidation of Cyclohexene Catalyzed by Nanoporous Au(Ag) in Liquid Phase, Catal. Letters. 147 (2017) 442–452. doi:10.1007/s10562-016-1883-6.
[24] B. Xu, C.G.F. Siler, R.J. Madix, C.M. Friend, Ag/Au Mixed Sites Promote Oxidative Coupling of Methanol on the Alloy Surface, Chem. - A Eur. J. 20 (2014) 4646–4652. doi:10.1002/chem.201304837.
[25] H. Shinotsuka, S. Tanuma, C.J. Powell, D.R. Penn, Calculations of electron inelastic mean free paths. X. Data for 41 elemental solids over the 50 eV to 200 keV range with the relativistic full Penn algorithm, Surf. Interface Anal. 47 (2015) 871–888. doi:10.1002/sia.5789.
[26] M.P. Seah, I.S. Gilmore, G. Beamson, XPS: Binding energy calibration of electron spectrometers 5—Re-evaluation of the reference energies, Surf. Interface Anal. 26 (1998) 642–649. doi:10.1002/(SICI)1096-9918(199808)26:9<642::AID-SIA408>3.0.CO;2-3.
[27] A.Y. Klyushin, T.C.R. Rocha, M. Hävecker, A. Knop-Gericke, R. Schlögl, A Near Ambient Pressure XPS Study of Au Oxidation, Phys. Chem. Chem. Phys. 16 (2014) 7881–7886.
[28] K.S. Kim, N. Winograd, X-ray photoelectron spectroscopic binding energy shifts due to matrix in alloys and small supported metal particles, Chem. Phys. Lett. 30 (1975) 91–95. doi:10.1016/0009-2614(75)85505-9.
[29] N. Kamiuchi, K. Sun, R. Aso, M. Tane, T. Tamaoka, H. Yoshida, S. Takeda, Self-Activated surface dynamics in gold catalysts under reaction environments, Nat. Commun. 9 (2018) 2060. doi:10.1038/s41467-018-04412-4.
[30] R.E. Watson, J. Hudis, M.L. Perlman, Charge Flow and *d* Compensation in Gold Alloys, Phys. Rev. B. 4 (1971) 4139–4144. doi:10.1103/PhysRevB.4.4139.

[31] M. Schmid, R.J. Madix, C.M. Friend, The creation of microscopic surface structures by interfacial diffusion of Au and Ag on Ag(110): A XPS and STM study, Surf. Sci. 643 (2016) 36–44. doi:10.1016/j.susc.2015.08.023.
[32] M.A. Van Spronsen, K.-J. Weststrate, A. Den Dunnen, M.E. Van Reijzen, C. Hahn, L.B.F. Juurlink, Hydrophilic Interaction between Low-Coordinated Au and Water: H_2O/Au(310) Studied with TPD and XPS, J. Phys. Chem. C. 120 (2016) 8693–8703. doi:10.1021/acs.jpcc.6b00912.
[33] M.A. Van Spronsen, K.-J. Weststrate, L.B.F. Juurlink, A Comparison of CO Oxidation by Hydroxyl and Atomic Oxygen from Water on Low-Coordinated Au Atoms, ACS Catal. 6 (2016) 7051–7058. doi:10.1021/acscatal.6b01720.
[34] P. Heimann, J.F. van der Veen, D.E. Eastman, Structure-Dependent Surface Core Level Shifts for the Au(111), (100), and (110) Surfaces, Solid State Commun. 38 (1981) 595–598. doi:http://dx.doi.org/10.1016/0038-1098(81)90947-9.
[35] M. Erbudak, P. Kalt, L. Schlapbach, K. Bennemann, Surface Core-Level Shifts at the End and Beginning of the Transition Metal Series, Surf. Sci. 126 (1983) 101–104. doi:http://dx.doi.org/10.1016/0039-6028(83)90698-2.
[36] A. Kafizas, S.A. Parry, A. V. Chadwick, C.J. Carmalt, I.P. Parkin, An EXAFS study on the photo-assisted growth of silver nanoparticles on titanium dioxide thin-films and the identification of their photochromic states, Phys. Chem. Chem. Phys. 15 (2013) 8254–8263. doi:10.1039/c3cp44513e.
[37] A.I. Frenkel, Applications of extended X-ray absorption fine-structure spectroscopy to studies of bimetallic nanoparticle catalysts, Chem. Soc. Rev. 41 (2012) 8163–8178. doi:10.1039/c2cs35174a.
[38] A.I. Frenkel, Q. Wang, S.I. Sanchez, M.W. Small, R.G. Nuzzo, Short range order in bimetallic nanoalloys: An extended X-ray absorption fine structure study, J. Chem. Phys. 138 (2013) 064202. doi:10.1063/1.4790509.
[39] C. Lakshmanan, A.K. Behera, R.N. Viswanath, S. Amirthapandian, R. Rajaraman, G. Amarendra, Microstructure studies in nanoporous Au: Effects on electro-oxidation, Scr. Mater. 146 (2018) 68–72. doi:10.1016/j.scriptamat.2017.11.018.
[40] T. Fujita, P. Guan, K. McKenna, X. Lang, A. Hirata, L. Zhang, T. Tokunaga, S. Arai, Y. Yamamoto, N. Tanaka, Y. Ishikawa, N. Asao, Y. Yamamoto, J. Erlebacher, M. Chen, Atomic origins of the high catalytic activity of nanoporous gold, Nat. Mater. 11 (2012) 775–780. doi:10.1038/nmat3391.
[41] T. Fujita, T. Tokunaga, L. Zhang, D. Li, L. Chen, S. Arai, Y. Yamamoto, A. Hirata, N. Tanaka, Y. Ding, M. Chen, Atomic Observation of Catalysis-Induced Nanopore Coarsening of Nanoporous Gold, Nano Lett. 14 (2014) 1172–1177. doi:10.1021/nl403895s.
[42] M.M. Montemore, R.J. Madix, E. Kaxiras, How Does Nanoporous Gold Dissociate Molecular Oxygen?, J. Phys. Chem. C. 120 (2016) 16636–16640. doi:10.1021/acs.jpcc.6b03371.
[43] J.L.C. Fajín, M.N.D.S. Cordeiro, J.R.B. Gomes, On the theoretical understanding of the unexpected O_2 activation by nanoporous gold, Chem. Commun. 47 (2011) 8403–8405. doi:10.1039/C1CC12166A.
[44] L. V Moskaleva, S. Röhe, A. Wittstock, V. Zielasek, T. Klüner, K.M. Neyman, M. Bäumer, Silver residues as a possible key to a remarkable oxidative catalytic activity of nanoporous gold., Phys. Chem. Chem. Phys. 13 (2011) 4529–4539. doi:10.1039/c0cp02372h.
[45] M.M. Montemore, E.D. Cubuk, J.E. Klobas, M. Schmid, R.J. Madix, C.M. Friend, E. Kaxiras, Controlling O coverage and stability by alloying Au and Ag, Phys. Chem. Chem. Phys. 18 (2016) 26844–26853. doi:10.1039/C6CP05611C.
[46] H. Shi, C. Stampfl, First-principles investigations of the structure and stability of oxygen adsorption and surface oxide formation at Au(111), Phys. Rev. B. 76 (2007) 075327. doi:10.1103/PhysRevB.76.075327.
[47] C. Barroo, M.M. Montemore, N. Janvelyan, B. Zugic, A.J. Akey, A.P. Magyar, J. Ye, E. Kaxiras, J. Biener, D.C. Bell, Macroscopic 3D Nanoporosity Formation by Dry Oxidation of AgAu Alloys, J. Phys. Chem. C. 121 (2017) 5115–5122. doi:10.1021/acs.jpcc.6b12847.
[48] L. Vitos, A.V. Ruban, H.L. Skriver, J. Kollár, The surface energy of metals, Surf. Sci. 411 (1998) 186–202. doi:10.1016/S0039-6028(98)00363-X.
[49] T.J.A. Slater, A. Macedo, S.L.M. Schroeder, M.G. Burke, P. O'Brien, P.H.C. Camargo, S.J. Haigh,

Correlating Catalytic Activity of Ag–Au Nanoparticles with 3D Compositional Variations, Nano Lett. 14 (2014) 1921–1926. doi:10.1021/nl4047448.
[50] Y. Li, W. Dononelli, R. Moreira, T. Risse, M. Bäumer, T. Klüner, L. V. Moskaleva, Oxygen-Driven Surface Evolution of Nanoporous Gold: Insights from Ab Initio Molecular Dynamics and Auger Electron Spectroscopy, J. Phys. Chem. C. 122 (2018) 5349–5357. doi:10.1021/acs.jpcc.7b08873.
[51] N. Gilis, L. Jacobs, C. Barroo, T. Visart de Bocarmé, Surface Segregation in Au–Ag Alloys Investigated by Atom Probe Tomography, Top. Catal. 61 (2018) 1437–1448. doi:10.1007/s11244-018-1040-0.
[52] T.A. Baker, X. Liu, C.M. Friend, The mystery of gold's chemical activity: local bonding, morphology and reactivity of atomic oxygen, Phys. Chem. Chem. Phys. 13 (2011) 34–46. doi:10.1039/C0CP01514H.
[53] J.L.C. Fajín, M.N.D.S. Cordeiro, J.R.B. Gomes, DFT study of the Au(3 2 1) surface reconstruction by consecutive deposition of oxygen atoms, Surf. Sci. 602 (2008) 424–435. doi:10.1016/j.susc.2007.10.037.
[54] L.C. Wang, Y. Zhong, D. Widmann, J. Weissmüller, R.J. Behm, Oxygen Adsorption and Low-Temperature CO Oxidation on a Nanoporous Au Catalyst: Reaction Mechanism and Foreign Metal Effects, Top. Catal. 61 (2018) 446–461. doi:10.1007/s11244-017-0881-2.
[55] L. V. Moskaleva, T. Weiss, T. Klüner, M. Bäumer, Chemisorbed Oxygen on the Au(321) Surface Alloyed with Silver: A First-Principles Investigation, J. Phys. Chem. C. 119 (2015) 9215–9226. doi:10.1021/jp511884k.
[56] G. Pia, E. Sogne, A. Falqui, F. Delogu, Ag surface segregation in nanoporous Au catalysts during CO oxidation, Sci. Rep. 8 (2018) 15208. doi:10.1093/gbe/evr001.
[57] L.C. Wang, Y. Zhong, D. Widmann, J. Weissmüller, R.J. Behm, On the Role of Residual Ag in Nanoporous Au Catalysts for CO Oxidation: A Combined Microreactor and TAP Reactor Study, ChemCatChem. 4 (2012) 251–259. doi:10.1002/cctc.201100297.
[58] G. Pia, A. Cincotti, F. Delogu, Thermally and catalytically induced coarsening of nanoporous Au, Mater. Lett. 183 (2016) 114–116. doi:10.1016/j.matlet.2016.07.051.
[59] T. Shirman, J. Lattimer, M. Luneau, E. Shirman, C. Reece, M. Aizenberg, R.J. Madix, J. Aizenberg, C.M. Friend, New Architectures for Designed Catalysts: Selective Oxidation using AgAu Nanoparticles on Colloid-Templated Silica, Chem. Eur. J. 24 (2018) 1833–1837. doi:10.1002/chem.201704552.